Efficiency / Power Density Analysis of Single-Phase and Three-Phase Transformers Employed in DAB and SRC DC/DC Converters

Type: Conference Proceedings

Authors:

Thomas Guillod, Daifei Zhang, Charles R. Sullivan, and Johann W. Kolar

Efficiency / Power Density Analysis of Single-Phase and Three-Phase Transformers Employed in DAB and SRC DC/DC Converters

Thomas Guillod*, Daifei Zhang†, Charles R. Sullivan*, and Johann W. Kolar‡

*Dartmouth College, Hanover NH, United States
†University of Toronto, Toronto, Canada
‡ETH Zürich, Zürich, Switzerland

Abstract—**This paper presents a comprehensive study of medium-frequency transformers used in single-phase and three-phase galvanically isolated DC/DC converters. The high-frequency core and winding losses are considered and the transformers are optimized with respect to the geometrical aspect ratios, the number of turns, and the frequency. The impact of the non-sinusoidal waveforms generated by the converters on the transformer losses is considered. The different transformers and converters are compared with both analytical and numerical methods. It is concluded that, for Dual-Active Bridge (DAB) and Series-Resonant (SRC) converters, the single-phase variants offer slightly more efficient (around 12% loss reduction for same overall volume) or compact (around 30% volume reduction for same losses) transformers than the three-phase variants.**

Index Terms—**Medium-frequency transformers, DC/DC power converters, three-phase electric power, dual-active bridge, optimization, scaling laws, open-source software.**

I. INTRODUCTION

Galvanically isolated DC/DC converters are indispensable in modern energy systems to match different voltage levels, block common-mode currents, confine ground faults, enhance modularity, and ensure end-user safety. This is especially true for emerging applications such as high-power electric vehicle charging, hydrogen electrolysis, integrated power electronics building blocks, and AI-centric data centers [1]–[5]. For high-power applications, both single-phase (see Fig. 1(a)) and three-phase (see Fig. 1(b)) isolated DC–DC converters are widely used, where Dual-Active-Bridge (DAB) and Series-Resonant (SRC) topologies are the dominant concepts [6]–[10]. In three-phase converters, the interleaved operation of the bridge-legs distributes the current across multiple phases, thereby reducing current stresses on active/passive components and easing filtering requirements [6], [7], [11].

For DC/DC converters, three main transformer configurations can be considered (see Fig. 2): a converter employing a single-phase transformer (1x1p), a three-phase converter with a star-connected three-phase transformer (1x3p), and a three-phase converter with three star-connected single-phase transformers (3x1p). The performance of the different combinations is a trade-off between several factors:

- The magnetic fluxes of three-phase transformers add up to zero, saving the need for a magnetic return path and reducing the volume of the magnetic core. This advantage is only applicable to the 1x3p configuration and not to the 3x1p configuration [6], [12].
- Three-phase converters generate smoother waveforms (fewer harmonics and reduced reactive power). This advantage is applicable to both the 1x3p and 3x1p configurations [6], [12], [13]
- Three-phase converters (1x3p and 3x1p) split the total power flow into three different coil sets. This is a disadvantage as low-power transformers are intrinsically less efficient than high-power designs [14]–[16].

However, a comprehensive comparative performance analysis of single-phase and three-phase transformers has rarely been carried out and the existing literature even reports conflicting findings [6], [7], [12], [17], [18]. Prior analyses do not consider the impact of the non-sinusoidal waveshapes on the core losses and the high-frequency winding losses [12], [17], [18]. Moreover, existing comparisons are often using a priori fixed variables (e.g., peak flux density, current density, and/or switching frequency), which might lead to suboptimal transformer designs [13], [17], [18].

In this paper, the three different transformer configurations (see Fig. 2) are compared for sinusoidal, DAB, and SRC excitations (see Fig. 3). The converters are operated with a constant voltage conversion ratio between the DC buses, i.e. as DC transformers (DCX). This paper is organized as follows.
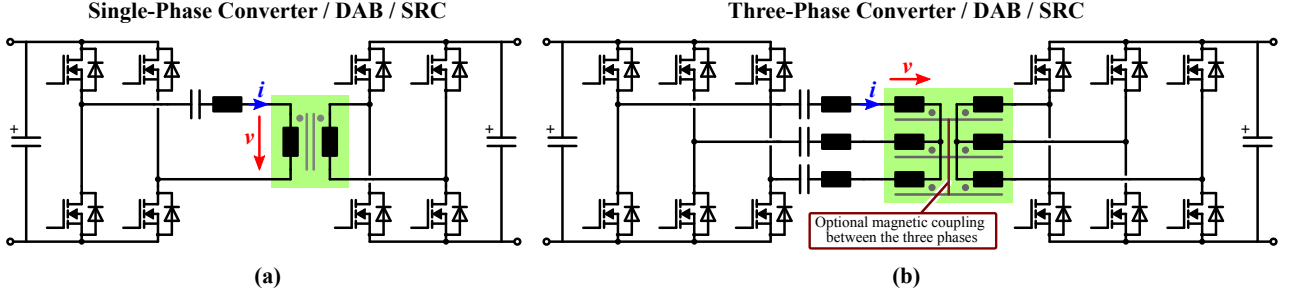
Fig. 1. (a) Single-phase DC/DC converters. (b) Three-phase DC/DC converters. External series inductors are used for the converter operation.

Each transformer is rated with one third of the total power.
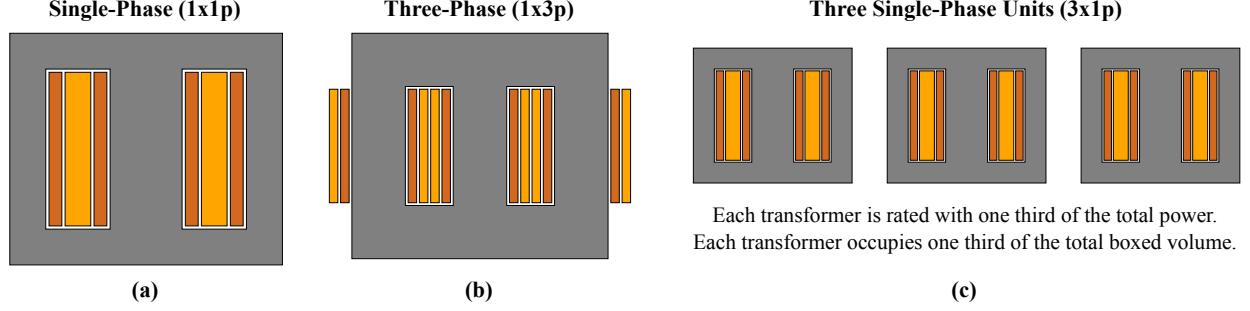Each transformer occupies one third of the total boxed volume.

Fig. 2. (a) Single-phase shell-type transformer. (b) Three-phase transformer. (c) Three single-phase transformers.
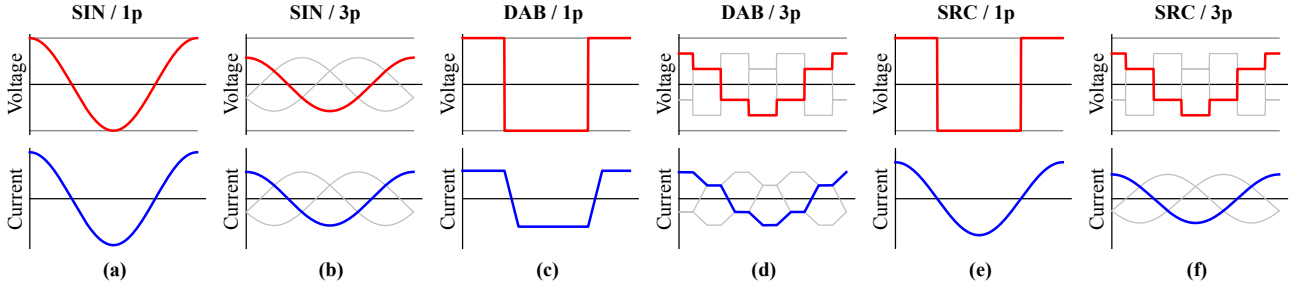

Fig. 3. (a)-(b) Sinusoidal waveforms. (c)-(d) DAB waveforms. (e)-(f) SRC waveforms. The magnetizing current of the transformers is neglected and the converters are operated with a fixed voltage conversion ratio between the DC buses (equal to the transformer voltage conversion ratio).

Section II introduces the transformer model (including the high-frequency losses and the impact of the non-sinusoidal waveforms) and defines the requirements for optimal designs. Section III provides general scaling laws with respect to the frequency, the power rating, the power density, the efficiency, the temperature, and the winding material. Section IV presents a general comparison methodology and benchmarks the transformer performance for the different converter topologies. Section V verifies the analytical expressions with a numerical global optimizer. The Python implementation of the proposed models and scaling laws is available under an open-source license [19], [20].

II. ANALYTICAL MODEL

In order to obtain general statements and scaling laws, several assumptions are required. The impact of the magnetizing and leakage inductances on the transformer operation is neglected

(external series inductors are used for the converter operation). The number of turns is represented by a continuous variable. The winding filling factor is assumed to be independent of the number of turns and the exact packing pattern of the turns is not considered. The presented model is applicable to both single-phase and three-phase transformers for sinusoidal and non-sinusoidal excitations. The different variables are defined in Tab. I.

A. Base Transformer Model

The peak flux density in the magnetic core can be expressed with the applied voltage, the frequency, the number of turns, and the core magnetic cross-section as [15], [21]

$$B_{\mathrm{pk}} = \frac{\kappa_{\mathrm{flux}}}{n A_{\mathrm{c}}} \frac{\sqrt{2} V_{\mathrm{rms}}}{2\pi f}, \tag{1}$$

TABLE I
VARIABLE DESCRIPTION

P	Transformer rated active power
ρ	Power density of the transformer
η	Efficiency of the transformer
P_{loss}	Total losses of the transformer
V_{rms}	RMS voltage applied to the windings
I_{rms}	RMS current in the windings
κ_{flux}	Core flux correction factor
κ_{igse}	Core loss correction factor
κ_{freq}	Winding frequency correction factor
λ_{trf}	Transformer power factor
n	Transformer number of turns
f	Transformer operating frequency
B_{pk}	Peak flux density in the magnetic core
P_{c}	Total core losses of the transformer
A_{c}	Cross-section of the magnetic core
V_{c}	Volume of the magnetic core
k_{i}	Core iGSE parameter
k_{c}	Core Steinmetz parameter
α_{c}	Core Steinmetz / iGSE parameter
β_{c}	Core Steinmetz / iGSE parameter
J_{rms}	RMS current density in the windings
r_{hf}	AC/DC winding resistance ratio
P_{w}	Total winding losses of the transformer
A_{w}	Cross-section of a single winding
V_{w}	Volume of all the windings
k_{w}	Winding filling factor
d_{s}	Winding strand diameter
d_{w}	Interleaving thickness
σ_{w}	Conductor material conductivity
ΔT	Transformer temperature rise
A_{t}	Exposed area for cooling
h_{t}	Surface convection coefficient

where κ_{flux} is an amplitude correction factor for non-sinusoidal waveforms. Then, the core losses can be computed with the core volume and the Steinmetz equation as [21], [22]

$$P_{\text{c}} = \left(\kappa_{\text{igse}} V_{\text{c}} \right) \left(k_{\text{c}} f^{\alpha_{\text{c}}} B_{\text{pk}}^{\beta_{\text{c}}} \right), \tag{2}$$

where κ_{igse} is a loss correction factor for non-sinusoidal waveforms based on the iGSE.

A litz wire winding is considered and the proximity losses are computed with a one-dimensional magnetic field distribution. The AC/DC resistance ratio can be expressed with the frequency, the strand diameter, the filling factor, the conductivity, and the winding thickness as [23]–[25]

$$r_{\text{hf}} = 1 + \frac{1}{12} \left(\pi \mu_0 \sigma_{\text{w}} k_{\text{w}} d_{\text{s}} d_{\text{w}} \right)^2 \left(\kappa_{\text{freq}} f \right)^2, \tag{3}$$

where κ_{freq} is a frequency correction factor for non-sinusoidal waveforms. The current density in the strands can be expressed with the applied current, the filling factor, and the winding cross-section as

$$J_{\text{rms}} = \frac{n}{k_{\text{w}} A_{\text{w}}} I_{\text{rms}}. \tag{4}$$

With the AC/DC resistance ratio, the current density, the filling factor, and the winding volume, the winding losses can be computed as

$$P_{\text{w}} = \left(k_{\text{w}} V_{\text{w}} r_{\text{hf}} \right) \frac{J_{\text{rms}}^2}{\sigma_{\text{w}}}. \tag{5}$$

The temperature rise of the transformer can be estimated with the transformer losses, the total exposed area, and the surface convection coefficient as

$$\Delta T = \frac{P_{\text{loss}}}{h_{\text{t}} A_{\text{t}}}. \tag{6}$$

This thermal model neglects the internal thermal resistances and the exact convection (free or forced) patterns.

B. Non-Sinusoidal Waveforms

For the flux density correction factor, a sinusoidal voltage (v_{sin}) with the same RMS value as the non-sinusoidal signal (v_{sig}) is first defined [13]:

$$v_{\text{sin}}(t) = V_{\text{rms}} \sqrt{2} \sin(2\pi f t). \tag{7}$$

The flux density in the core is proportional to the integral of the applied voltage. The peak-to-peak values of the non-sinusoidal signal and the equivalent sinusoidal signal can be computed as

$$B(t) \propto \int_0^t v(\tau)\, \text{d}\tau, \tag{8}$$

$$B_{\text{pkpk}} = \max(B(t)) - \min(B(t)). \tag{9}$$

Then, the correction factor for the flux density produced by a non-sinusoidal voltage with respect to a sinusoidal voltage with an identical RMS value can be extracted as

$$\kappa_{\text{flux}} = \frac{B_{\text{pkpk,sig}}}{B_{\text{pkpk,sin}}}. \tag{10}$$

The flux density correction factor is only dependent on the waveshape. The factor does not depend on the frequency, the amplitude, or the other transformer parameters.

The core losses are not only impacted by the peak flux density but also by the waveshape of the flux density. The corresponding core loss correction factor can be computed with the iGSE [21], [22]. The losses are computed for both the non-sinusoidal and the sinusoidal flux densities

$$p_{\text{igse}} = f \int_0^T k_{\text{i}} B_{\text{pkpk}}^{\beta_{\text{c}} - \alpha_{\text{c}}} \left| \frac{\text{d}B(\tau)}{\text{d}\tau} \right|^{\alpha_{\text{c}}} \text{d}\tau. \tag{11}$$

Then, the correction factor for the core loss produced by a non-sinusoidal flux density with respect to a sinusoidal flux density with an identical peak-to-peak value can be extracted with the loss ratio as

$$\kappa_{\text{igse}} = \frac{1}{\kappa_{\text{flux}}^{\beta_{\text{c}}}} \frac{p_{\text{igse,sig}}}{p_{\text{igse,sin}}}. \tag{12}$$

The core loss correction factor is only dependent on the waveshape and the Steinmetz coefficient α_{c}. The factor does not depend on the frequency, the amplitude, the Steinmetz parameter β_{c}, the Steinmetz parameter k_{c}, the iGSE parameter k_{i}, or the other transformer parameters.

For the winding frequency correction factor, a sinusoidal current (i_{sin}) with the same RMS value as the non-sinusoidal signal (i_{sig}) is first defined:

$$i_{\text{sin}}(t) = I_{\text{rms}} \sqrt{2} \sin(2\pi f t). \tag{13}$$

The proximity losses in the strands are proportional to the square of the frequency [23]. In the time domain, the proximity losses are proportional to the square of the derivative of the magnetic flux density and the average eddy current losses can be expressed as [26]

$$p_{\text{prox}} \propto f \int_0^T \left(\frac{\text{d}i(\tau)}{\text{d}\tau} \right)^2 \text{d}\tau. \tag{14}$$

Then, the correction factor between the effective frequency and the fundamental frequency for a non-sinusoidal current can be expressed as

$$\kappa_{\text{freq}} = \sqrt{\frac{p_{\text{prox,sig}}}{p_{\text{prox,sin}}}}. \tag{15}$$

The winding frequency correction factor is only dependent on the waveshape. The factor does not depend on the frequency, the amplitude, or the other transformer parameters.

C. Transformer Optimization

In order to obtain a fair comparison between the converter topologies, only optimized transformers should be considered. The selection of the number of turns and the number of turns is a trade-off between the core and winding losses. The minimum losses are reached under the following condition [13], [15]:

$$n = n_{\text{opt}} \Leftrightarrow \frac{P_{\text{c}}}{P_{\text{w}}} = \frac{2}{\beta_{\text{c}}}. \tag{16}$$

The number of turns is adapted in order to meet a constant ratio between the core and the winding losses. This implies that, besides practical fabrication constraints, the transformer performance is independent of the voltage transfer ratio (primary to secondary) and the ratio between the voltage and the current (terminal impedance).
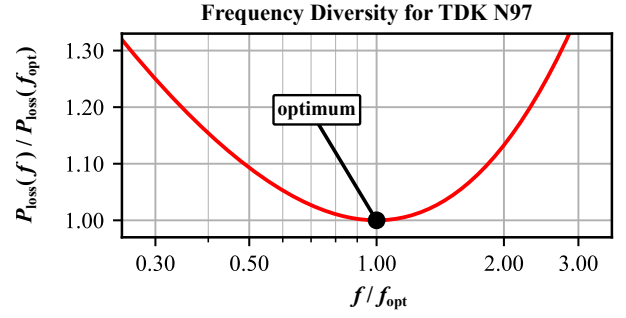

Fig. 4. Sensitivity of the losses with respect to the operating frequency (also called frequency diversity) for TDK N97.

The performance of magnetic components generally improves with the frequency. However, beyond a certain frequency, the high-frequency winding losses rapidly increase and limit the achievable performance [27]. The following condition can be extracted for the optimal operating frequency [15], [24]:

$$f = f_{\text{opt}} \Leftrightarrow r_{\text{hf}} = \frac{\beta_{\text{c}}}{\alpha_{\text{c}}}. \tag{17}$$

It should be noted that the compatibility of the optimal operating point with the material limitations (saturation flux density, maximum frequency, loss density, etc.) should be checked. Medium-frequency transformers using ferrite cores and litz wire windings are typically operated significantly below the saturation limit and the aforementioned optima are valid [15], [24], [28].

III. TRANSFORMER SCALING LAWS

With the optimal frequency and the optimal number of turns, the general behavior of transformers across frequency, power rating, power density, and winding type can be described with scaling laws. The scaling laws only depend on the Steinmetz parameters α_{c} and β_{c}.

A. Steinmetz Parameters

In this paper, the MnZn ferrite material TDK N97 is selected [29]. The Steinmetz parameters are extracted from the manufacturer loss data with a c [30]:

- Core temperature: $80\,^{\circ}\text{C}$
- Frequency: $[100 - 300]\,\text{kHz}$
- Flux density: $[30 - 130]\,\text{mT}$
- Loss density: $[5 - 500]\,\text{mW/cm}^3$
- Fitted values: $k_{\text{c}} = 0.039$, $\alpha_{\text{c}} = 1.72$, and $\beta_{\text{c}} = 2.46$
- Error: $\text{avg} = 2.6\,\%$, $\text{rms} = 3.3\,\%$, and $\text{max} = 12.3\,\%$

The fitting range has been selected with respect to the typical operating points of optimal MF transformers ($10\,\text{kW}$ power rating). For such transformers, the optimal operating points are compatible with the Steinmetz parameter fitting ranges.

TABLE II
POWER AND VOLUME SCALING LAWS

$P = $ constant	$\rho = $ constant	$1 - \eta = $ constant	$\Delta T = $ constant
$\rho = $ variable	$P = $ variable	$P = $ variable	$P = $ variable
$1-\eta \propto \rho^{+\frac{2\alpha_c+3\beta_c-6}{3\beta_c+6}} \propto \rho^{+0.36}$	$1-\eta \propto P^{-\frac{2\alpha_c}{3\beta_c+6}} \propto P^{-0.26}$	$\rho \propto P^{+\frac{2\alpha_c}{2\alpha_c+3\beta_c-6}} \propto P^{+0.71}$	$\rho \propto P^{-\frac{\beta_c-2\alpha_c+2}{2\alpha_c+5\beta_c-2}} \propto P^{-0.07}$
$\Delta T \propto \rho^{\frac{2\alpha_c+5\beta_c-2}{3\beta_c+6}} \propto \rho^{+1.03}$	$\Delta T \propto P^{+\frac{\beta_c-2\alpha_c+2}{3\beta_c+6}} \propto P^{+0.08}$	$\Delta T \propto P^{+\frac{\beta_c+2\alpha_c-2}{2\alpha_c+3\beta_c-6}} \propto P^{+0.81}$	$1-\eta \propto P^{-\frac{\beta_c+2\alpha_c-2}{2\alpha_c+5\beta_c-2}} \propto P^{-0.28}$
$f \propto \rho^{+\frac{1}{3}} \propto \rho^{+0.33}$	$f \propto P^{-\frac{1}{3}} \propto P^{-0.33}$	$f \propto P^{-\frac{\beta_c-2}{2\alpha_c+3\beta_c-6}} \propto P^{-0.10}$	$f \propto P^{-\frac{2\beta_c}{2\alpha_c+5\beta_c-2}} \propto P^{-0.36}$

TABLE III
WINDING MATERIAL SCALING LAWS

$P = $ constant	$P = $ constant	$P = $ constant	$P = $ constant
$\rho = $ constant	$\rho = $ constant	$\rho = $ constant	$\rho = $ constant
$\sigma_w = $ variable	$k_w = $ variable	$d_s = $ variable	$d_w = $ variable
$1-\eta \propto \sigma_w^{-\frac{2\alpha_c-\beta_c}{\beta_c+2}} \propto \sigma_w^{-0.22}$	$1-\eta \propto k_w^{-\frac{2\alpha_c-\beta_c}{\beta_c+2}} \propto k_w^{-0.22}$	$1-\eta \propto d_s^{+\frac{2\beta_c-2\alpha_c}{\beta_c+2}} \propto d_s^{+0.33}$	$1-\eta \propto d_w^{+\frac{2\beta_c-2\alpha_c}{\beta_c+2}} \propto d_w^{+0.33}$
$\Delta T \propto \sigma_w^{-\frac{2\alpha_c-\beta_c}{\beta_c+2}} \propto \sigma_w^{-0.22}$	$\Delta T \propto k_w^{-\frac{2\alpha_c-\beta_c}{\beta_c+2}} \propto k_w^{-0.22}$	$\Delta T \propto d_s^{+\frac{2\beta_c-2\alpha_c}{\beta_c+2}} \propto d_s^{+0.33}$	$\Delta T \propto d_w^{+\frac{2\beta_c-2\alpha_c}{\beta_c+2}} \propto d_w^{+0.33}$
$f \propto \sigma_w^{-1} \propto \sigma_w^{-1.00}$	$f \propto k_w^{-1} \propto k_w^{-1.00}$	$f \propto d_s^{-1} \propto d_s^{-1.00}$	$f \propto d_w^{-1} \propto d_w^{-1.00}$

B. Frequency Diversity

An important property of medium-frequency transformers is the sensitivity of the losses with respect to the operating frequency [15]. If a suboptimal frequency and an optimal number of turns are selected, the impact of the suboptimal frequency on the losses can be expressed independently of the power density and the power rating as

$$\frac{P_{\text{loss}}(f)}{P_{\text{loss}}(f_{\text{opt}})} = \left(\frac{f^2}{f_{\text{opt}}^2}\right)^{\frac{\alpha_c}{2+\beta_c}} \left(1 - \frac{\alpha_c}{\beta_c} + \frac{\alpha_c}{\beta_c}\frac{f_{\text{opt}}^2}{f^2}\right)^{\frac{\beta_c}{2+\beta_c}} . \quad (18)$$

For TDK N97, the frequency diversity is shown in Fig. 4. For this material, the frequency can be increased or decreased by a factor of two with respect to the optimum with less than 15 % additional losses. For converter optimization, this implies that the optimal frequency of the complete converter system can be significantly different than the transformer optimal frequency [31].

C. Power and Volume Scaling Laws

Exponential scaling laws can be derived for transformers operated at the optimal frequency with the optimal number of turns. The transformer volume is scaled with fixed geometrical aspect ratios (homothetic scaling). All the other parameters (core material, strand diameter, filling factor, etc.) are kept constant. Tab. II depicts the scaling laws for four different cases: scaling at constant power, constant power density, constant efficiency, and constant temperature [14], [15]. The numerical values for TDK N97 are also reported.

The following general trends can be observed. Transformers with higher power density are less efficient and feature increased temperatures and operating frequencies. High-power transformers are intrinsically more efficient and feature increased temperatures. Therefore, beyond a certain power, transformers will be thermally limited. With a constant temperature, low-power transformers are more compact but also less efficient.

D. Winding Material Scaling Laws

The impact of the winding conductivity, filling factor, and stranding on the performance can also be described with scaling laws, as shown in Tab. III. The numerical values for TDK N97 are also reported. The increased losses associated with lower conductivities and filling factors are mitigated by the increased penetration depth for the eddy currents.

This implies that an aluminum winding with 60 % of the copper conductivity will only increase the losses by 12 %. Increasing the filling factor by 50 % will only lead to a 9 % loss reduction. Increasing the strand diameter by 50 % will increase the losses by 14 %. Reducing the winding thickness by a factor of two (interleaving of the primary and secondary coils) will reduce the losses by 21 % (the impact of the interleaving on the achieved filling factor is neglected in this analysis).

TABLE IV
TRANSFORMER CONFIGURATION / LOSSES

Type	Figure	Loss factor	$\frac{y_{\text{window}}}{x_{\text{window}}}$	$\frac{z_{\text{limb}}}{x_{\text{limb}}}$	$\frac{A_{\text{core}}}{A_{\text{window}}}$
1x1p	Fig. 2(a)	1.00	3.00	3.54	5.34
1x3p	Fig. 2(b)	1.28	3.00	3.15	1.77
3x1p	Fig. 2(c)	1.33	3.00	3.54	5.34

IV. TRANSFORMERS FOR DC/DC CONVERTERS

All the results presented in the previous sections (loss models, optimal frequency, optimal number of turns, frequency diversity, and scaling laws) are valid for all medium-frequency transformer configurations (see Fig. 2) and converter topologies (see Fig. 3). Therefore, the impact of the transformer configuration and converter topology can be examined independently of the power rating and power density.

A. Impact of the Transformer Configuration

The transformer geometry can be described with a few variables: the boxed volume (V_{box}), the core volume (V_{c}), the core area (A_{c}), the winding volume (V_{w}), the winding area (A_{w}), and the winding thickness (d_{w}). For optimal transformers (optimal frequency and optimal number of turns), the losses are found to be proportional to

$$P_{\text{loss}} \propto \left(\xi^{2\beta_{\text{c}}} P^{2\beta_{\text{c}}} \frac{V_{\text{c}}^2}{A_{\text{c}}^{2\beta_{\text{c}}}} \frac{V_{\text{w}}^{\beta_{\text{c}}}}{A_{\text{w}}^{2\beta_{\text{c}}}} \frac{d_{\text{w}}^{2\beta_{\text{c}}}}{d_{\text{w}}^{2\alpha_{\text{c}}}} \right)^{\frac{1}{2+\beta_{\text{c}}}}, \quad (19)$$

where P is the power rating of the transformer. The factor ξ accounts for the different current loading of the winding window for single-phase ($\xi = 2$ for 1x1p and 3x1p) and three-phase transformers ($\xi = 2/3$ for 1x3p).

With this expression, the performance of single-phase and three-phase transformers (see Fig. 2) can be compared for TDK N97. The geometrical aspect ratios of the transformer can be optimized for each transformer configuration with a constant boxed volume. It should be noted that an unconstrained optimization generates an extremely narrow winding window in order to limit the proximity losses. Therefore, due to practical fabrication constraints, the aspect ratio of the winding window is limited to 3.00. The losses of the different transformer configurations are reported in Tab. IV and the optimal geometries are shown in Fig. 5. The loss values are normalized with respect to the single-phase transformer and are independent of the power rating and the power density (as long as the transformers are not thermally constrained).

Contrary to a common misconception, one full-power single-phase transformer outperforms three-phase designs (loss factor of 1.28). As expected, using three single-phase transformers is suboptimal (loss factor of 1.33). This last factor can also be derived from the scaling laws with a constant power density

Single-Phase (1x1p / 3x1p)   **Three-Phase (1x3p)**
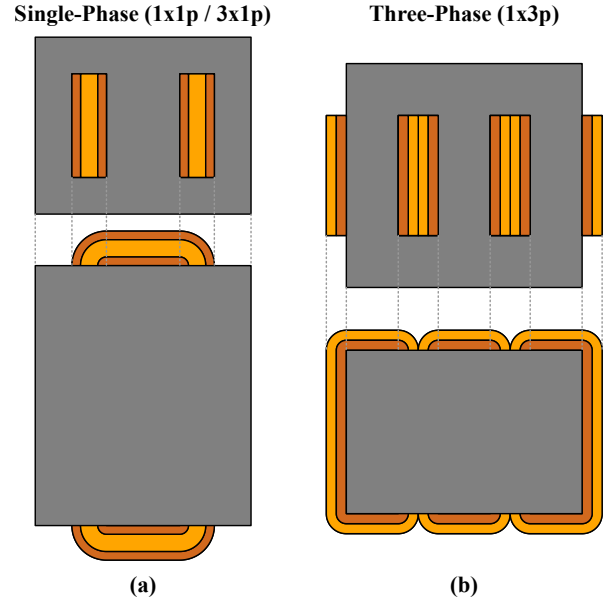

(a)   **(b)**

Fig. 5. Optimal geometry (aspect ratios) for (a) single-phase and (b) three-phase transformers (see Tab. IV).

that predicts that low-power transformers are less efficient than high-power designs (see Tab. II):

$$\frac{1 - \eta_{\text{3x1p}}}{1 - \eta_{\text{1x1p}}} = \left(\frac{P_{\text{3x1p}}}{P_{\text{1x1p}}} \right)^{-\frac{2\alpha_{\text{c}}}{3\beta_{\text{c}}+6}} = \left(\frac{1}{3} \right)^{-0.26} = 1.33. \quad (20)$$

B. Impact of the Converter Topology

Single-phase and three-phase converters (see Fig. 3) operate with different waveshapes and, therefore, different transformer losses. The transformer ratings are proportional to the apparent power and, therefore, the power factor is a critical parameter for assessing the performance:

$$\lambda_{\text{trf}} = \frac{P}{\zeta V_{\text{rms}} I_{\text{rms}}}, \quad (21)$$

where ζ is the number of phases in the transformer ($\zeta = 1$ for 1x1p and 3x1p) and three-phase transformers ($\zeta = 3$ for 1x3p). For optimal transformers (optimal frequency and optimal number of turns), the losses are found to be proportional to

$$P_{\text{loss}} \propto \left(\kappa_{\text{flux}}^{2\beta_{\text{c}}} \kappa_{\text{igse}}^2 \frac{\kappa_{\text{freq}}^{2\beta_{\text{c}}}}{\kappa_{\text{freq}}^{2\alpha_{\text{c}}}} \frac{1}{\lambda_{\text{trf}}^{2\beta_{\text{c}}}} \right)^{\frac{1}{2+\beta_{\text{c}}}}. \quad (22)$$

For TDK N97, the DAB and SRC converters are compared to pure sinusoidal excitations. A phase shift of $30°$ is used for the DAB topologies. The losses of the different converter types are reported in Tab. V. The loss values are normalized with respect to the sinusoidal waveforms and are independent of the power rating and the frequency. It can be seen that SRC converters outperform DAB converters due to the sinusoidal resonant current. Three-phase converters generate better waveforms

TABLE V
CONVERTER TOPOLOGY / LOSSES

Type	Figure	Loss factor	κ_{flux}	κ_{igse}	κ_{freq}	λ_{trf}
SIN / 1p	Fig. 3(a)	1.00	1.00	1.00	1.00	1.00
SIN / 3p	Fig. 3(b)	1.00	1.00	1.00	1.00	1.00
DAB / 1p	Fig. 3(c)	1.43	1.11	0.87	1.65	0.88
DAB / 3p	Fig. 3(d)	1.26	1.05	0.93	1.41	0.91
SRC / 1p	Fig. 3(e)	1.18	1.11	0.87	1.00	0.90
SRC / 3p	Fig. 3(f)	1.07	1.05	0.93	1.00	0.95

TABLE VI
TRANSFORMER COMPARISON

Type	Type	$\left.\frac{P_{\text{loss}}}{P_{\text{best}}}\right|V_{\text{box}} = \text{const}$	$\left.\frac{V_{\text{box}}}{V_{\text{best}}}\right|P_{\text{loss}} = \text{const}$
1x1p	SIN / 1p	$1.00 \times 1.00 = 1.00$	$1.00^{2.77} = 1.00$
1x1p	DAB / 1p	$1.00 \times 1.43 = 1.43$	$1.43^{2.77} = 2.68$
1x1p	SRC / 1p	$1.00 \times 1.18 = 1.18$	$1.18^{2.77} = 1.60$
1x3p	SIN / 3p	$1.28 \times 1.00 = 1.28$	$1.28^{2.77} = 1.98$
1x3p	DAB / 3p	$1.28 \times 1.26 = 1.62$	$1.62^{2.77} = 3.79$
1x3p	SRC / 3p	$1.28 \times 1.07 = 1.38$	$1.38^{2.77} = 2.42$
3x1p	SIN / 3p	$1.33 \times 1.00 = 1.33$	$1.33^{2.77} = 2.19$
3x1p	DAB / 3p	$1.33 \times 1.26 = 1.68$	$1.68^{2.77} = 4.19$
3x1p	SRC / 3p	$1.33 \times 1.07 = 1.42$	$1.42^{2.77} = 2.67$

than their single-phase counterparts for both DAB and SRC operations. It should be noted that the comparison is done with a fixed voltage conversion ratio between the DC buses, i.e., DCX operation. However, the presented analysis method is also applicable to Buck/Boost operating modes.

C. Comparison of DC/DC Converters

It appears that single-phase transformers are advantageous for the transformer itself (see Tab. IV) and three-phase converters generate better waveforms (see Tab. V). The total transformer performance inside the converter (transformer losses with a fixed volume and power rating) is obtained by multiplying the aforementioned loss factors. Alternatively, the volume of the transformers can be compared with constant losses using the exponential scaling laws (see Tab. II) between the efficiency and the power density:

$$\rho \propto (1 - \eta)^{+\frac{3\beta_c + 6}{2\alpha_c + 3\beta_c - 6}} \propto (1 - \eta)^{+2.77}. \tag{23}$$

Tab. VI shows the obtained loss and volume factors for TDK N97. It can be concluded that, from a transformer perspective, single-phase converters offer slightly better performance than three-phase converters for both DAB and SRC operations. Using three single-phase transformers instead of a single three-phase transformer is suboptimal. The derived factors are independent of the power rating and power density. For three-phase converters, it is also possible to connect the transformer in a delta configuration [8]. It has been found that, for DCX operations, the star/wye and delta configurations feature similar performance.

V. NUMERICAL RESULTS

The aforementioned analysis is verified with a full numerical optimization. TDK N97 is selected as a core material and a litz wire winding is used. The main parameters and constraints are summarized in Tab. VII. A evolutionary algorithm is used to optimize the transformer volume, the aspect ratios, the frequency, and the number of turns. A continuous variable is used for the number of turns in order to obtain smooth curves. The different design constraints (saturation flux, frequency, loss density, minimum distance, thermal limit, etc.) are enforced

TABLE VII
DESIGN VARIABLES

k_c	0.039	Core Steinmetz parameter
α_c	1.72	Core Steinmetz parameter
β_c	2.46	Core Steinmetz parameter
B_{max}	200 mT	Max. flux density
f_{max}	400 kHz	Max core op. frequency
p_{max}	500 mW/cm^3	Max. core loss density
k_w	25 %	Winding filling factor
d_s	71 μm	Winding strand diameter
σ_w	46 MS/m	Copper conductivity
J_{max}	6 A/mm^2	Max. current density
f_{max}	800 kHz	Max. winding op. frequency
p_{max}	500 mW/cm^3	Max. winding loss density
d_{iso}	1 mm	Coil insulation distance
h_t	20 W/m^2/K	Surface convection coefficient
ΔT_{max}	80 °C	Maximum temperature rise

during the optimization. The power rating is set to 10 kW and the converters are operated between two 600 V DC-buses.

Tab. VIII shows the transformer losses and the optimal operating frequencies obtained with a power density of 20 kW/dm^3. Tab. IX depicts the transformer volumes and the optimal operating frequencies obtained with a transformer efficiency of 99.8 %. The loss and volume factors are in good agreement with the value reported in Tab. VI, proving the validity of the analytical models.

Fig. 6 depicts the transformer losses at different frequencies for DAB and SRC converters. Due to the current harmonics, DAB converters employ lower optimal operating frequencies and exhibit higher losses. The optimal frequencies of the single-phase transformers (1x1p) and the three-phase (1x3p) transformers are similar. However, the single-phase transformers feature lower losses. The configurations with three single-phase transformers have higher operating frequencies and higher losses, as predicted by the scaling laws. As expected,
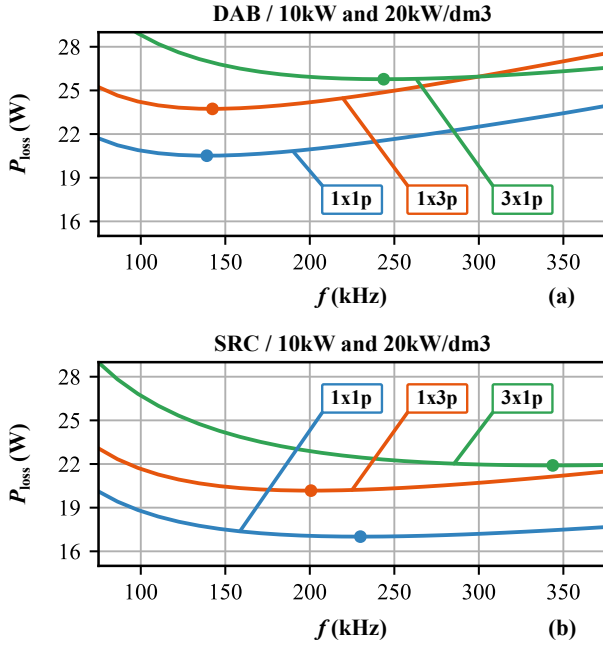
Fig. 6. Transformer losses for different operating frequencies for (a) DAB and (b) SRC converters ($10\,\text{kW}$, $600\,\text{V}$, and $20\,\text{kW/dm}^3$).

TABLE VIII
RESULTS / FIXED VOLUME / $10\,\text{kW}$ / $20\,\text{kW/dm}^3$

Type	Type	Losses	Frequency	Loss Factor
1x1p	SIN / 1p	14.4 W	230.4 kHz	1.00
1x1p	DAB / 1p	20.5 W	139.1 kHz	1.43
1x1p	SRC / 1p	17.0 W	230.3 kHz	1.18
1x3p	SIN / 3p	18.8 W	200.8 kHz	1.31
1x3p	DAB / 3p	23.7 W	142.3 kHz	1.65
1x3p	SRC / 3p	20.2 W	200.6 kHz	1.40
3x1p	SIN / 3p	20.4 W	343.8 kHz	1.42
3x1p	DAB / 3p	25.8 W	243.7 kHz	1.79
3x1p	SRC / 3p	21.9 W	343.4 kHz	1.52

the sensitivity of the transformer losses with respect to the frequency is low (see Fig. 4).

Fig. 7 depicts the transformer losses at different power densities for DAB and SRC converters. As predicted by the analytical models, the trends between the transformer configurations and converter topologies are independent of the power density. It can also be observed that using a constant and suboptimal switching frequency has a limited impact on the achieved efficiency.

VI. CONCLUSION

This paper presents a comprehensive analysis of the transformer performance for single-phase and three-phase DC/DC converters, including the impact of the high-frequency losses and the non-sinusoidal waveforms. It is found that the advantageous waveforms of three-phase converters (fewer harmonics,

TABLE IX
RESULTS / FIXED EFFICIENCY / $10\,\text{kW}$ / $99.8\,\%$

Type	Type	Volume	Frequency	Volume Factor
1x1p	SIN / 1p	$227.0\,\text{cm}^3$	306.8 kHz	1.00
1x1p	DAB / 1p	$531.5\,\text{cm}^3$	136.2 kHz	2.34
1x1p	SRC / 1p	$338.1\,\text{cm}^3$	265.3 kHz	1.49
1x3p	SIN / 3p	$430.3\,\text{cm}^3$	211.7 kHz	1.90
1x3p	DAB / 3p	$755.7\,\text{cm}^3$	122.5 kHz	3.33
1x3p	SRC / 3p	$510.3\,\text{cm}^3$	199.1 kHz	2.25
3x1p	SIN / 3p	$523.0\,\text{cm}^3$	338.2 kHz	2.30
3x1p	DAB / 3p	$904.4\,\text{cm}^3$	195.8 kHz	3.99
3x1p	SRC / 3p	$617.1\,\text{cm}^3$	317.7 kHz	2.72

higher power factor, etc.) are not sufficient to compensate for the increased losses of three-phase transformers. Therefore, from a transformer perspective, single-phase DC/DC converters outperform the three-phase variants. Furthermore, for DCX operations, SRC converters feature lower transformer losses than DAB converters.

However, the selection of the optimal transformer also depends on practical constraints (e.g., commercially available parts, fabrication complexity, placement of the terminals, thermal management). Furthermore, besides the transformer, the different converter topologies feature different advantages for the other passive and active components (e.g., capacitors, soft-switching, control). Therefore, the presented analysis is necessary, but not sufficient for obtaining an optimized converter system.

SOURCE CODE

The source code used to generate the presented results is available under an open-source license [19], [20]. The transformer model, analytical optima, scaling laws, converter excitations, and numerical optimization routines are implemented in Python using NumPy, SciPy, and Matplotlib.

The source code includes the following transformer types: single-phase shell-type, single-phase core-type, and three-phase. The waveforms produced by DAB and SRC converters are included for the following converter topologies: single-phase converters, three-phase converters with a star/wye connection, and three-phase converters with a delta connection. The fitting code for the Steinmetz parameters is also included.
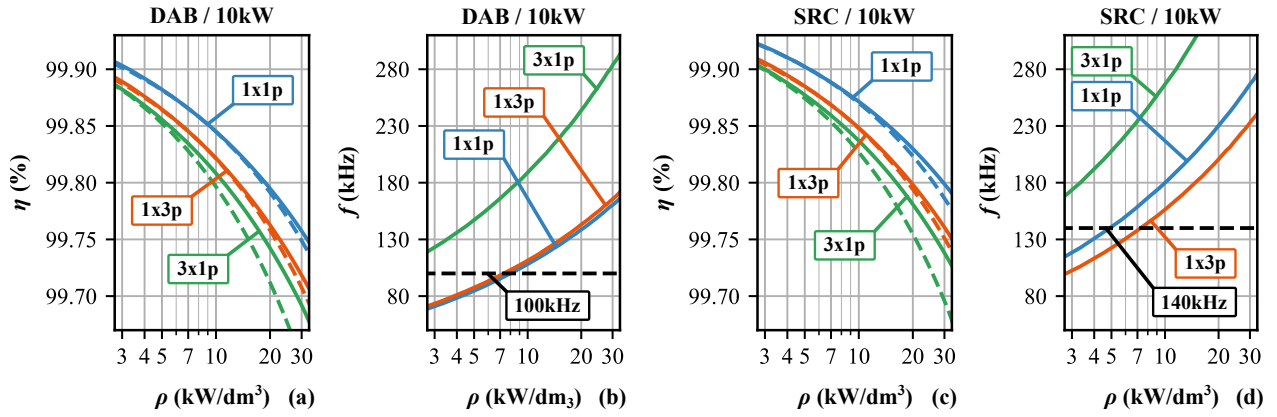
Fig. 7. (a) Transformer efficiencies and (b) optimal frequencies for DAB converters (10 kW and 600 V). (c) Transformer efficiencies and (d) operating frequencies for SRC converters (10 kW and 600 V). The solid curves depict the frequency-optimized designs. The dashed curves show frequency-constrained designs (100 kHz for DAB and 140 kHz for SRC).

REFERENCES

[1] C. Blaum, J. Pfeiffer, C. Drexler, and M. Schmidhuber, "A Ferrite Transformer Design for a Medium Voltage High Power Charging System," in *Proc. of the Int. Exhibition and Conference on Power Electronics, Intelligent Motion, Renewable Energy, and Energy Management (PCIM)*, 2025.

[2] I. Khan, S. Rahman, M. A. Ayaz, M. Amir, and H. Shehada, "Review of Isolated DC-DC Converters for Application in Data Center Power Delivery," *IEEE Transactions on Industry Applications*, vol. 60, no. 4, pp. 5436–5446, 2024.

[3] X. Li, K. G. Ravikumar, and C. Peabody, "±400 V DC Rack For AI/ML Applications," in *Proc. of the Open Compute Project (OCP) Global Summit*, 2024.

[4] M. Lawson, T. Moaz, N. Rajagopal, V. Mitrovic, D. Dong, and C. DiMarino, "Model-Based Design and Analysis of a Navy Integrated Power Electronics Building Block (NiPEBB)," *IEEE Transactions on Transportation Electrification*, vol. 10, no. 4, pp. 7816–7827, 2024.

[5] M. Chen, S. Chou, F. Blaabjerg, and P. Davari, "Overview of Power Electronic Converter Topologies Enabling Large-Scale Hydrogen Production via Water Electrolysis," *Applied Sciences*, vol. 12, no. 4, pp. 1–12, 2022.

[6] R. W. A. A. De Doncker, D. M. Divan, and M. H. Kheraluwala, "A Three-Phase Soft-Switched High-Power-Density DC/DC Converter for High-Power Applications," *IEEE Transactions on Industry Applications*, vol. 27, no. 1, pp. 63–73, 1991.

[7] U. Mustafa, I. Kougioulis, A. J. Watson, P. Wheeler, and M. R. Ahmed, "Design Analysis of High-Frequency, High Power 3-Phase DAB Transformer for Electric Vehicle Charger Applications," in *Proc. of the IEEE Transportation Electrification Conference and Expo (ITEC)*, 2024.

[8] B. H. Baars, J. Everts, C. G. E. Wijnands, and E. A. Lomonova, "Performance Evaluation of a Three-Phase Dual Active Bridge DC–DC Converter with Different Transformer Winding Configurations," *IEEE Transactions on Power Electronics*, vol. 31, no. 10, pp. 6814–6823, 2016.

[9] F. Schwarz, "A Method of Resonant Current Pulse Modulation for Power Converters," *IEEE Transactions on Industrial Electronics and Control Instrumentation*, vol. IECI-17, no. 3, pp. 209–221, 1970.

[10] W. Mcmurray, "Multipurpose Power Converter Circuits," 1969, US Patent 3,487,289.

[11] D. Zhang, P. Sbabo, D. Biadene, P. Mattavelli, and J. W. Kolar, "Novel Isolated-Three-Phase-HF-Link Matrix-Type Three-Phase AC/DC Converter (i3X-Rectifier)," in *Proc. IEEE Workshop Control Model. Power Electron. (COMPEL)*, 2025.

[12] J. Xue, F. Wang, D. Boroyevich, and Z. Shen, "Single-Phase vs. Three-Phase High Density Power Transformers," in *Proc. of the IEEE Energy Conversion Congress and Exposition (ECCE USA)*, 2010.

[13] W. G. Hurley, W. H. Wolfle, and J. G. Breslin, "Optimized Transformer Design: Inclusive of High-Frequency Effects," *IEEE Transactions on Power Electronics*, vol. 13, no. 4, pp. 651–659, 1998.

[14] C. R. Sullivan, B. A. Reese, A. L. F. Stein, and P. A. Kyaw, "On Size and Magnetics: Why Small Efficient Power Inductors are Rare," in *Proc. of the IEEE Int. Symposium on 3D Power Electronics Integration and Manufacturing (3D-PEIM)*, 2016.

[15] T. Guillod and J. W. Kolar, "Medium-Frequency Transformer Scaling Laws: Derivation, Verification, and Critical Analysis," *IEEE CPSS Transactions on Power Electronics and Applications*, vol. 5, no. 1, pp. 18–33, 2020.

[16] A. Arruti, J. Anzola, I. Aizpuru, and M. Mazuela, "Single Core and Modular Transformer Solutions: A Trade-Off Analysis of Volume, Losses and Temperature Rise," in *Proc. of the IEEE Annual Conf. of the Industrial Electronics Society (IECON)*, 2022.

[17] J. Xue, "Single-Phase vs. Three-Phase High Power High Frequency Transformers," Ph.D. dissertation, Virginia Tech, 2010.

[18] C. P. Dick, A. Konig, and R. W. De Doncker, "Comparison of Three-Phase DC-DC Converters vs. Single-Phase DC-DC Converters," in *Proc. of the IEEE Int. Conference on Power Electronics and Drive Systems (PEDS)*, 2007.

[19] T. Guillod. (2025) PyScaleXFMR - Optimization and Scaling of Medium-Frequency Transformers. GitHub. [Online]. Available: https://github.com/otvam/pyscalexfmr

[20] T. Guillod. (2025) PyScaleXFMR - Optimization and Scaling of Medium-Frequency Transformers. Zenodo. [Online]. Available: https://doi.org/10.5281/zenodo.17288902

[21] C. C. Valchev and A. Van den Bossche, *Inductors and Transformers for Power Electronics*. CRC press, 2018.

[22] K. Venkatachalam, C. R. Sullivan, T. Abdallah, and H. Tacca, "Accurate Prediction of Ferrite Core Loss with Nonsinusoidal Waveforms Using Only Steinmetz Parameters," in *Proc. of the IEEE Workshop on Computers in Power Electronics (CIPE)*, 2002.

[23] C. Sullivan, "Optimal Choice for Number of Strands in a Litz-Wire Transformer Winding," *IEEE Transactions on Power Electronics*, vol. 14, no. 2, pp. 283–291, 1999.

[24] M. Leibl, G. Ortiz, and J. W. Kolar, "Design and Experimental Analysis of a Medium-Frequency Transformer for Solid-State Transformer Applications," *IEEE Journal of Emerging and Selected Topics in Power Electronics*, vol. 5, no. 1, pp. 110–123, 2017.

[25] J. A. Ferreira, *Electromagnetic Modelling of Power Electronic Converters*. Springer Science & Business Media, 1989.

[26] C. Sullivan, "Computationally Efficient Winding Loss Calculation with Multiple Windings, Arbitrary Waveforms, and Two-Dimensional or Three-Dimensional Field Geometry," *IEEE Transactions on Power Electronics*, vol. 16, no. 1, pp. 142–150, 2001.

[27] A. J. Hanson, J. A. Belk, S. Lim, C. R. Sullivan, and D. J. Perreault, "Measurements and Performance Factor Comparisons of Magnetic Materials at High Frequency," *IEEE Transactions on Power Electronics*, vol. 31, no. 11, pp. 7909–7925, 2016.

[28] E. Ng, A. Brown, and A. J. Hanson, "Magnetic Scaling and Constraints," in *Proc. of the IEEE Applied Power Electronics Conf. and Expo. (APEC)*, 2025.

[29] TDK Electronics, "Ferrites And accessories: SIFERRIT material N97," Jun. 2025.

[30] TDK Electronics, "Ferrite Magnetic Design Tool v6.0," Feb. 2024.

[31] J. W. Kolar, D. Bortis, and D. Neumayr, "The Ideal Switch is Not Enough," in *Proc. of the IEEE Int. Symposium on Power Semiconductor Devices and ICs (ISPSD)*, 2016.